

Suspended Tissue Open Microfluidic Patterning (STOMP)

Supplementary Information

Amanda J. Haack^{1,2*}, Lauren G. Brown^{1*}, Alex J. Goldstein^{3,4,5}, Priti Mulimani^{3,6}, Jean Berthier¹, Asha R. Viswanathan¹, Irina Kopyeva⁷, Jamison M. Whitten¹, Ariel Lin^{1,8}, Serena H. Nguyen¹, Thomas P. Leahy^{3,9}, Ella E. Bouker¹, Ruby M. Padgett^{3,9}, Natalie A. Mazzawi^{3,6,10}, Jodie C. Tokihiro¹, Ross C. Bretherton^{3,7}, Aaliyah Wu¹, Stephen J. Tapscott^{11,12}, Cole A. DeForest^{1,3,7,8,13,14}, Tracy E. Popowics^{3,6}, Erwin Berthier¹, Nathan J. Sniadecki^{3,5,7,9#}, Ashleigh B. Theberge^{1,15#}

*Authors contributed equally to this work

#Corresponding authors: Nathan J. Sniadecki, nsniadec@uw.edu & Ashleigh B. Theberge, abt1@uw.edu

Affiliations:

1. Department of Chemistry, University of Washington, Seattle, WA, 98195 USA
2. Medical Scientist Training Program, University of Washington School of Medicine, Seattle, WA, 98195 USA
3. Institute for Stem Cell & Regenerative Medicine, University of Washington, Seattle, WA, 98109 USA
4. Department of Materials Science and Engineering, University of Washington, Seattle, WA, 98195 USA.
5. Department of Laboratory Medicine & Pathology, University of Washington, Seattle, WA, 98195 USA
6. Oral Health Sciences, School of Dentistry, University of Washington, Seattle, WA, 98195 USA
7. Department of Bioengineering, University of Washington, Seattle, WA, 98195 USA
8. Molecular Engineering & Sciences Institute, University of Washington, Seattle, WA, 98109 USA
9. Department of Mechanical Engineering, University of Washington, Seattle, WA, 98195 USA
10. Department of Microbiology, University of Washington, Seattle, WA, 98195 USA
11. Human Biology Division, Fred Hutchinson Cancer Center, Seattle, WA 98109, USA
12. Department of Neurology, University of Washington, Seattle WA 98195, USA
13. Department of Chemical Engineering, University of Washington, Seattle, WA, 98195 USA
14. Institute for Protein Design, University of Washington, Seattle, WA, 98195 USA
15. Department of Urology, University of Washington School of Medicine, Seattle, WA, 98195 USA

The PDF file includes:

- Supplementary Figures S1 to S13
- Supplementary Tables S1 to S3
- Supplementary Methods
- Supplementary Text
- Supplementary References 1-9

Other Supplementary Information for this manuscript include the following:

Supplementary videos:

- Supplementary video 1: 3 region STOMP patterning with agarose (Fig. 1)
- Supplementary videos 2a-d: Experimental pinning videos (Fig. 2)
- Supplementary video 3: D14 STOMP EHT beating unpaced GFP (Fig. 3)
- Supplementary video 4: D14 STOMP EHT beating unpaced mCherry (Fig. 3)
- Supplementary video 5: Patterning degradable wall geometry with agarose (Fig. 5)
- Supplementary video 6: Removing PEG tissue after degrading walls (Fig. 5)

STL Files: Contact corresponding authors for design files for STOMP devices shown in this work.

Supplementary Figures

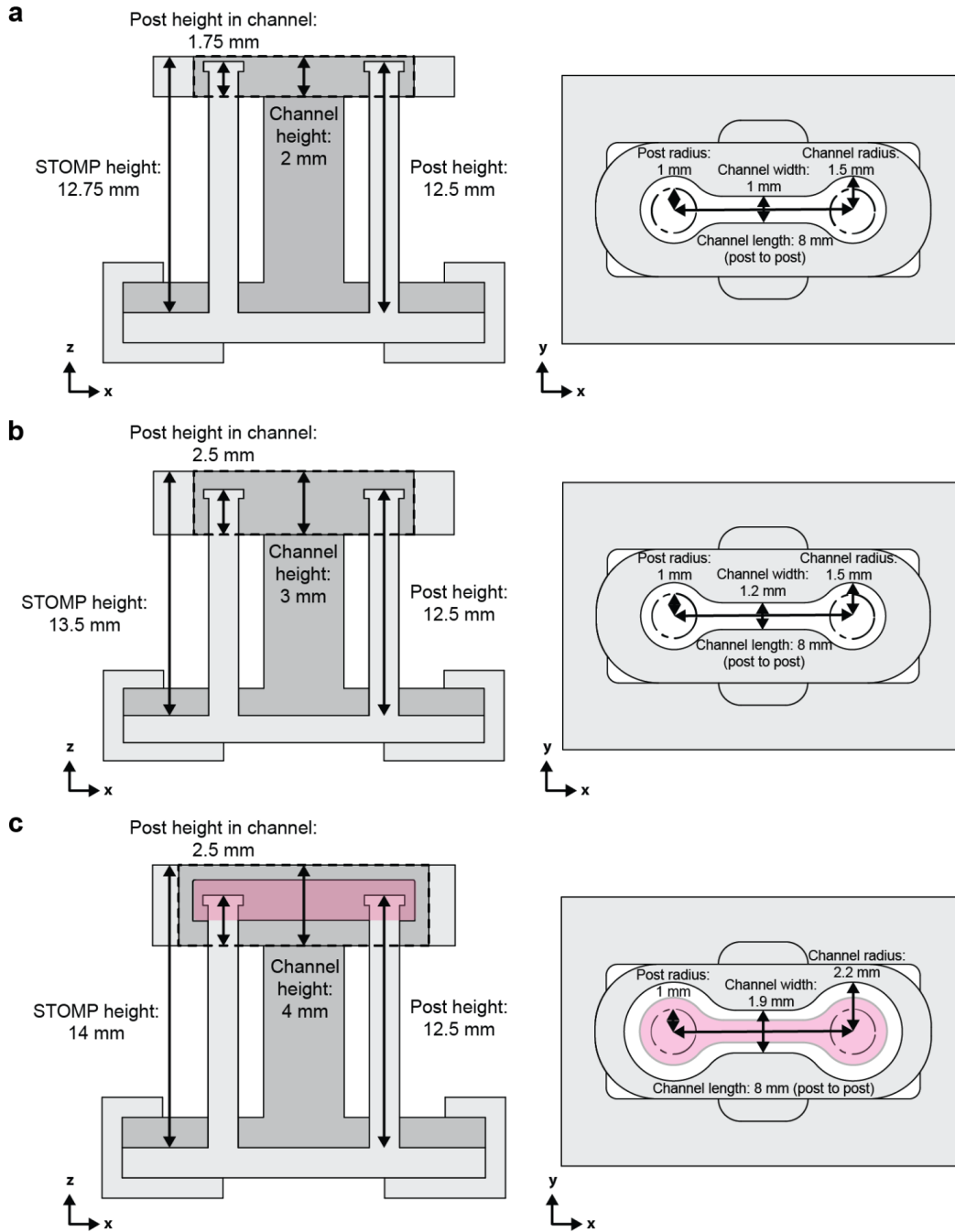


Figure S1. Dimensions of STOMP devices used in this work. a) 2 mm height device, b) 3.5 mm height device, and c) outer region patterning device surrounding previously patterned hydrogel (in pink), featured in Fig. 5.

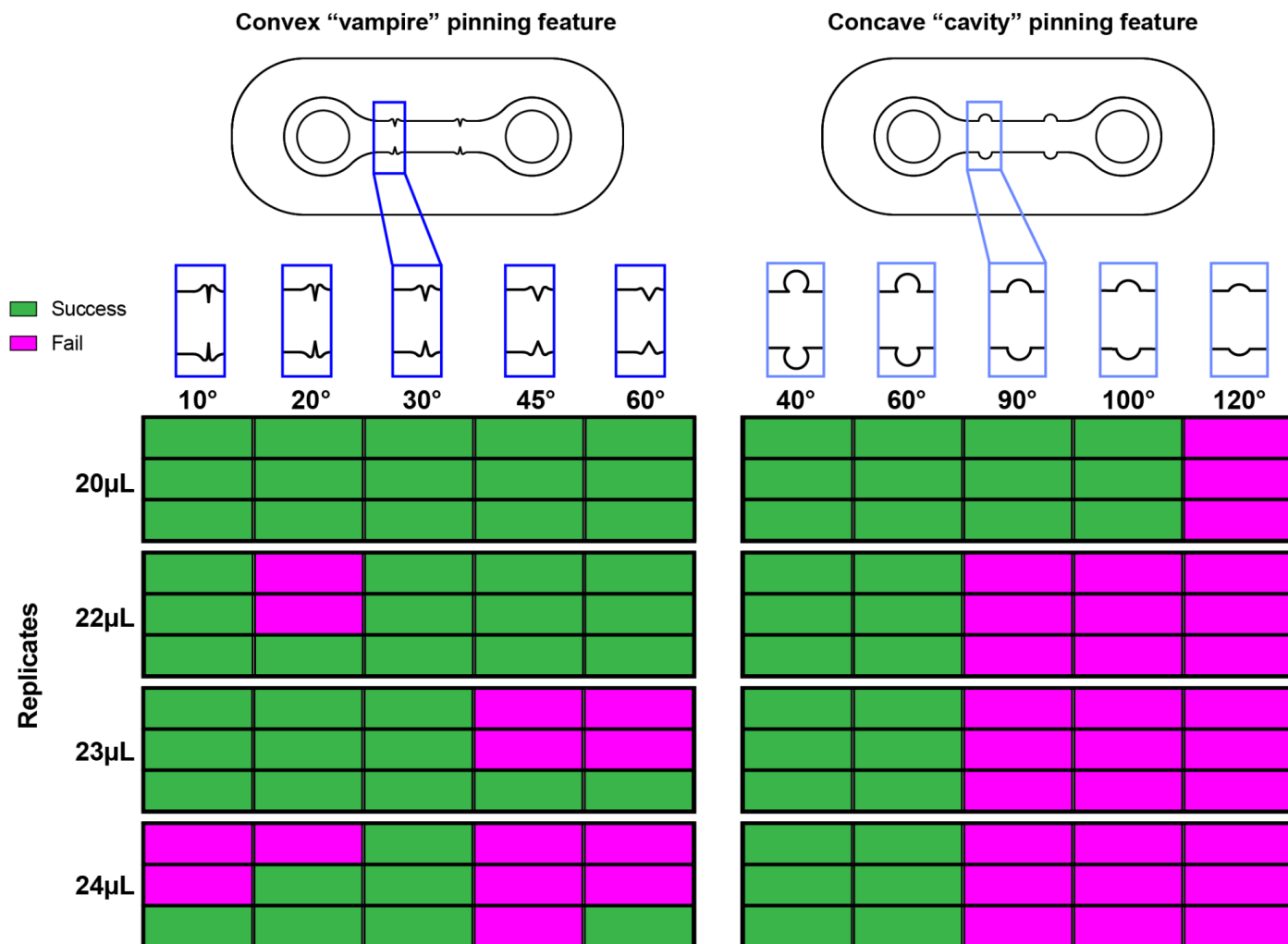


Figure S2. Experimental results of pinning of the 5 mg/mL collagen precursor fluid front at different pipetted volumes. For both the convex "vampire" and concave "cavity" pinning features, five different pinning feature angles were tested to observe either success (green) or failure (magenta) of pinning at the pinning feature. For the convex "vampire" pinning features, the angle of the pinning feature refers to the vertex angle of the triangular pinning feature. For the concave "cavity" pinning features, the angle of pinning feature refers to the angle between the line tangent to the semicircular pinning feature to the straight channel wall.

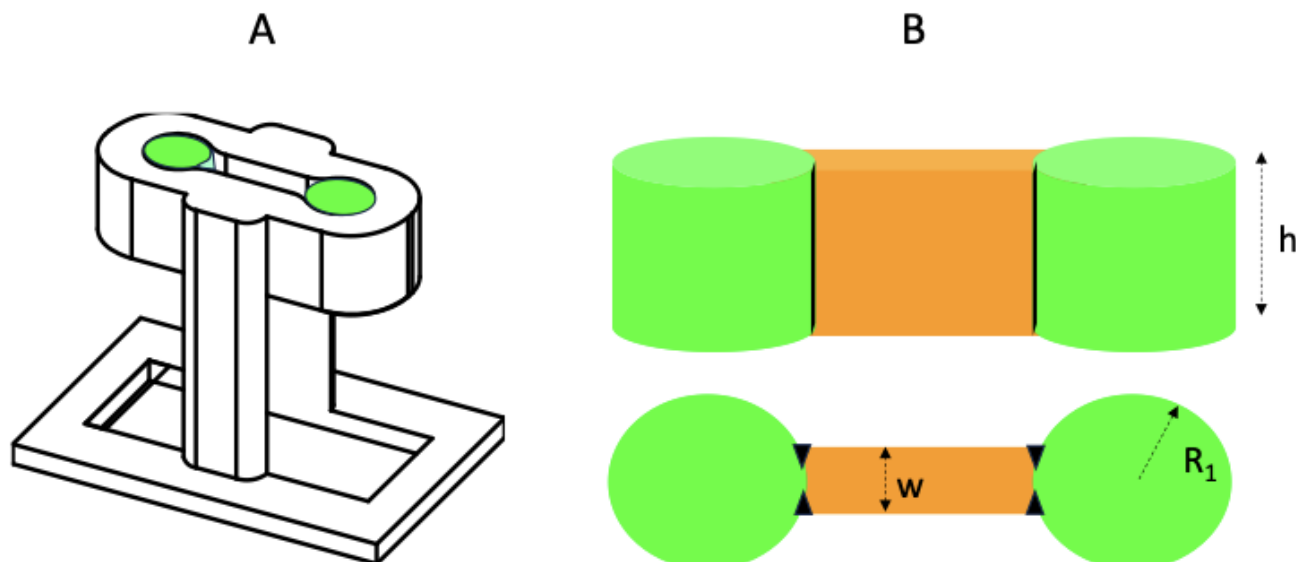


Figure S3. Modeling fluid in the multi region STOMP device. A) isometric view of the device. B) top: side view of the filled device; bottom: top view of the filled device. The black lines and arrows symbolize the relief/design that pins the liquids during the filling.

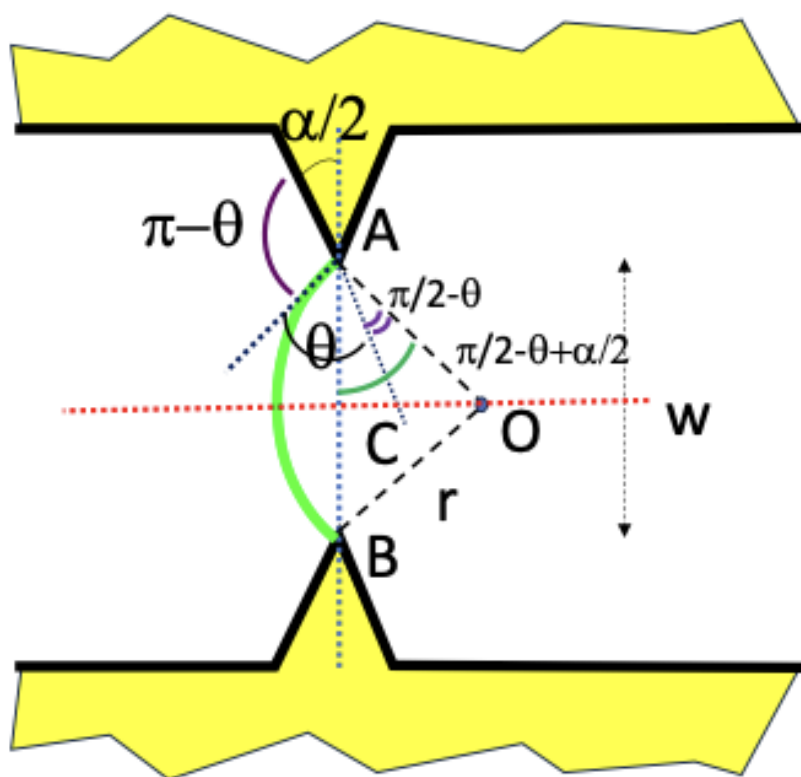


Figure S4. Geometrical analysis of convex “vampire” pinning features. Green line is the fluid front, where the hydrogel precursor was pipetted first into the region on the right, so the fluid front is bulging to the left at the Laplace pinning threshold.

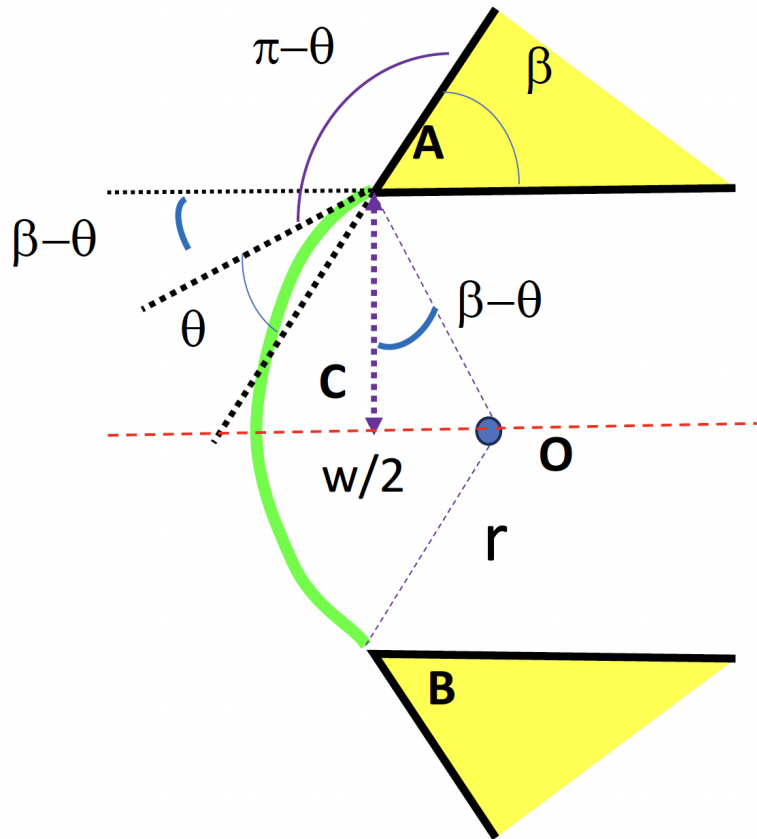


Figure S5. Geometrical analysis of concave “cavity” pinning features when $\beta > \theta$. Green line is the fluid front, where the hydrogel precursor was pipetted first into the region on the right, so the fluid front is bulging to the left at the Laplace pinning threshold.

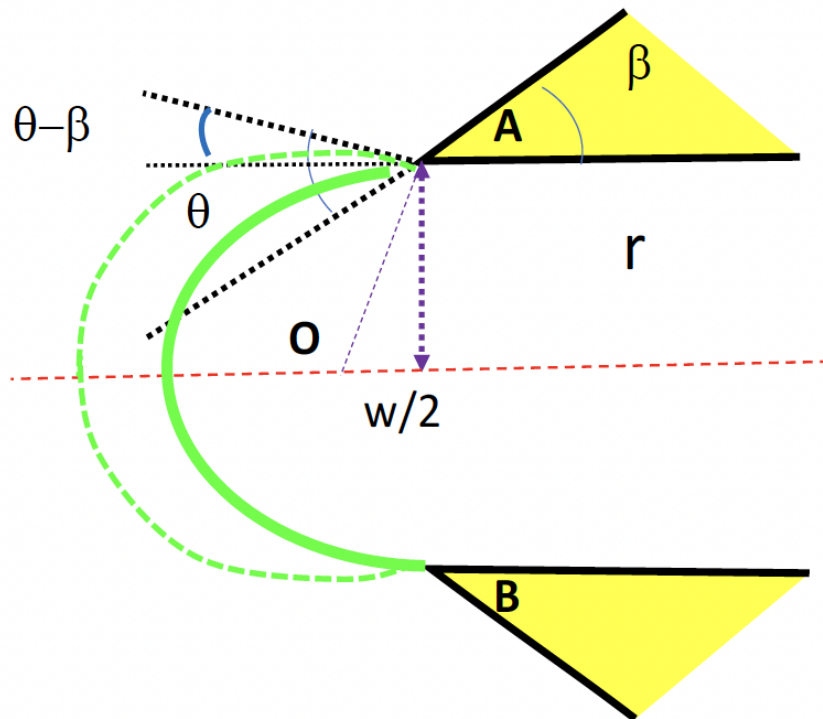


Figure S6. Geometrical analysis of concave “cavity” pinning features when $\beta < \theta$. The dotted green line is the expected fluid front, where the hydrogel precursor was pipetted first into the region on the right, so the fluid front is bulging to the left. However, the actual fluid front is the solid green line, which is the maximum Laplace pinning threshold.

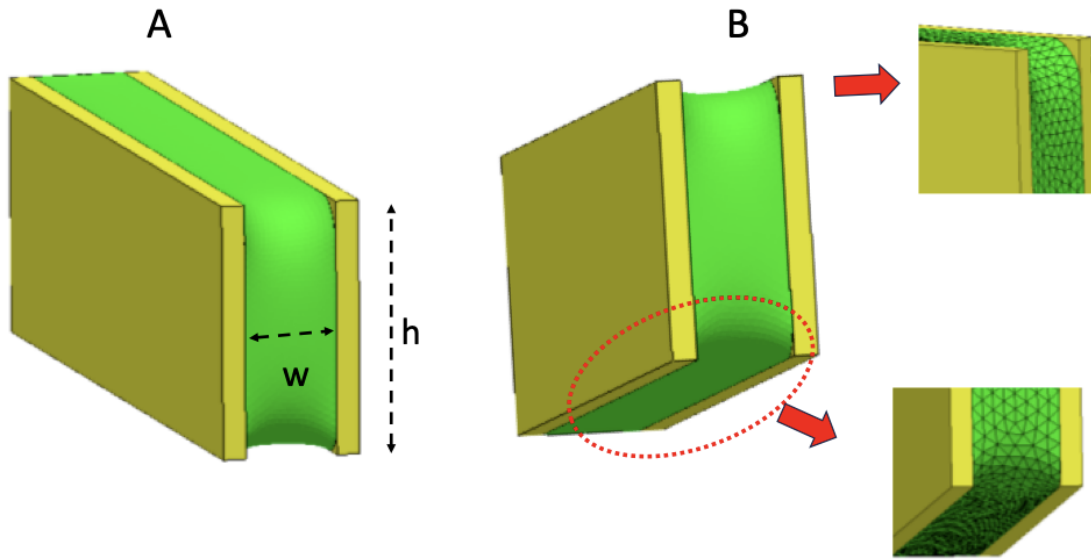


Figure S7. 3D calculation of the free air-liquid interface of a liquid between two vertical walls with a width of 1.2 mm and a height of 3.5 mm. A) Isometric view of a fluid (green) within an open channel with two walls and no ceiling or floor. B) Closer view of the top and bottom corners of the vertical interface, showing the plots obtained using the Surface Evolver software.

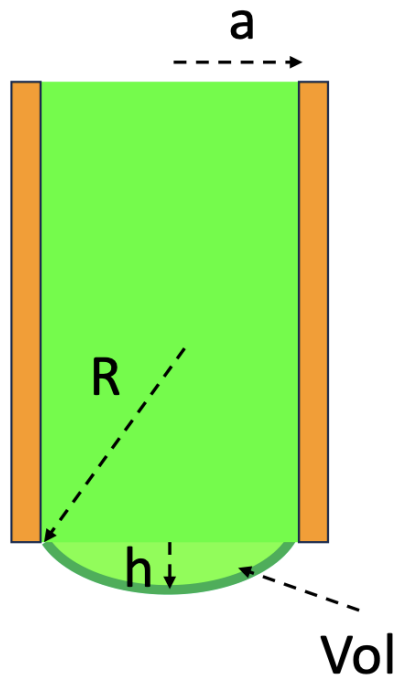


Figure S8. Schematic of the fluid (green) bulging below the suspended channel walls (orange).

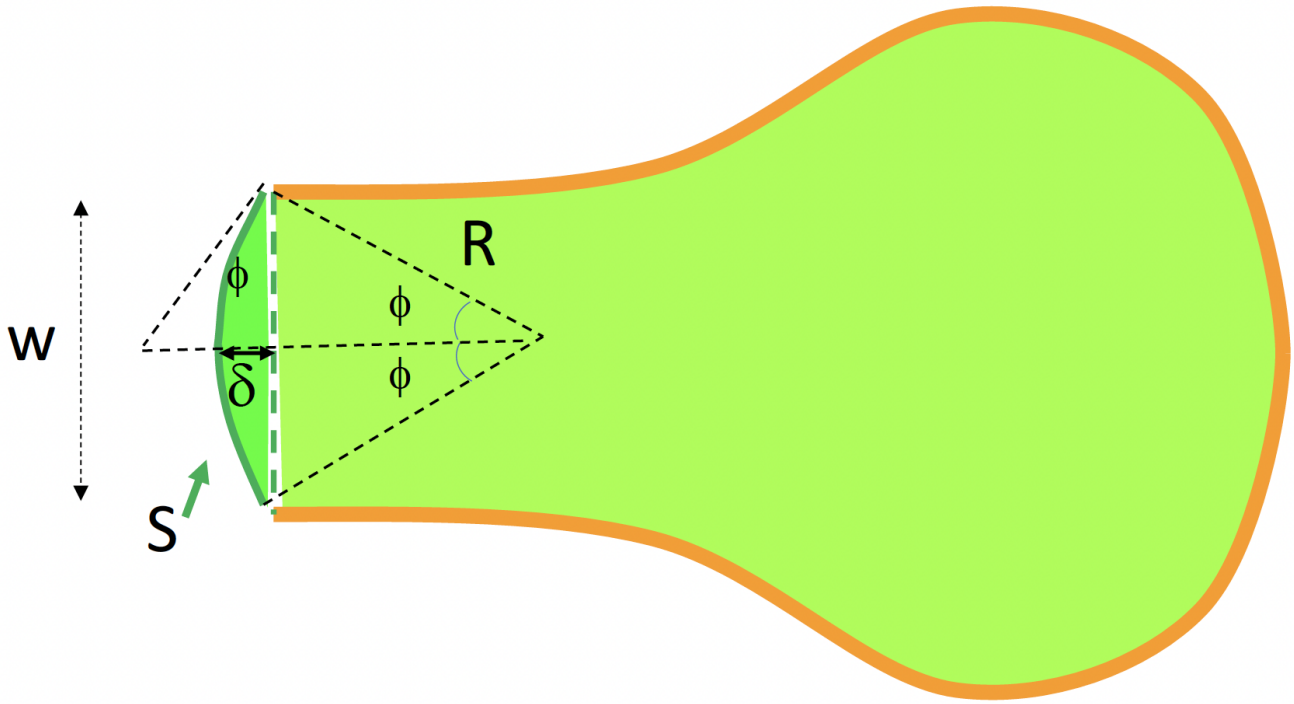


Figure S9. Top-down schematic of the fluid (green) filling the outer regions of the suspended channel (walls denoted in orange) before reaching the pinning features (location marked by dotted green line). After reaching the pinning feature, the fluid will bulge some distance δ along the vertical interface, with the bulging angle denoted as ϕ . The surface area S (dark green) is the surface area of the bulging liquid along the vertical interface.

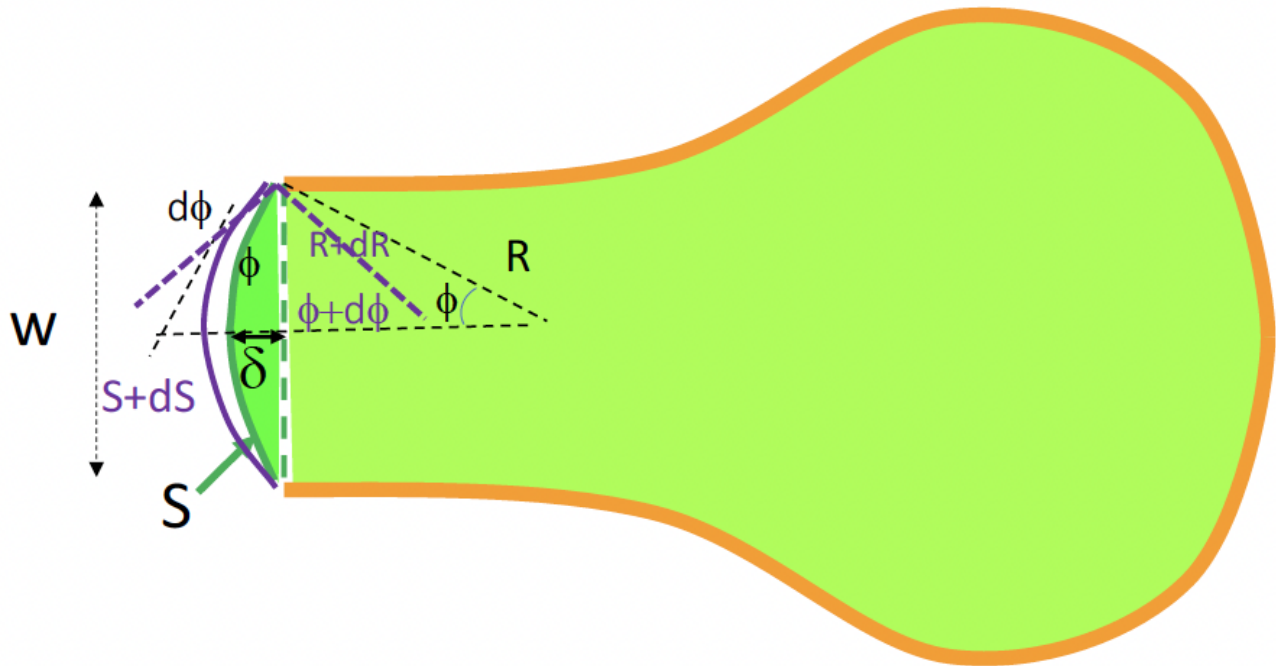


Figure S10. Top-down schematic of how the bulging fluid (dark green) along the vertical interface changes after pipetting additional volume into the suspended channel.

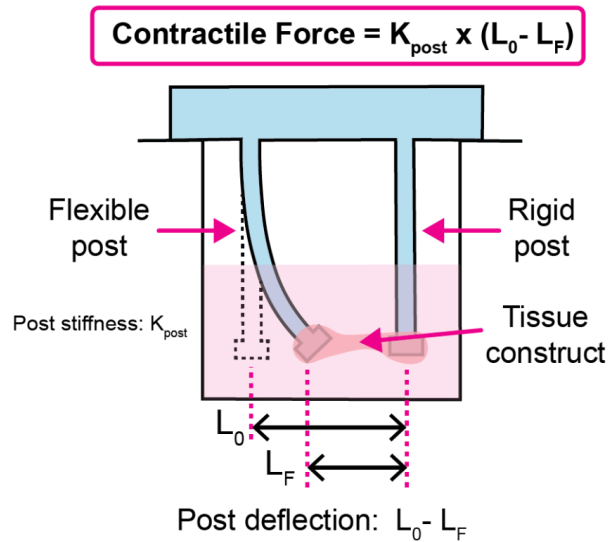


Figure S11. Tissue contractile force calculation using post deflection. Deflection of post is measured by initial length of tissue, L_0 , minus the final length of tissue, L_F

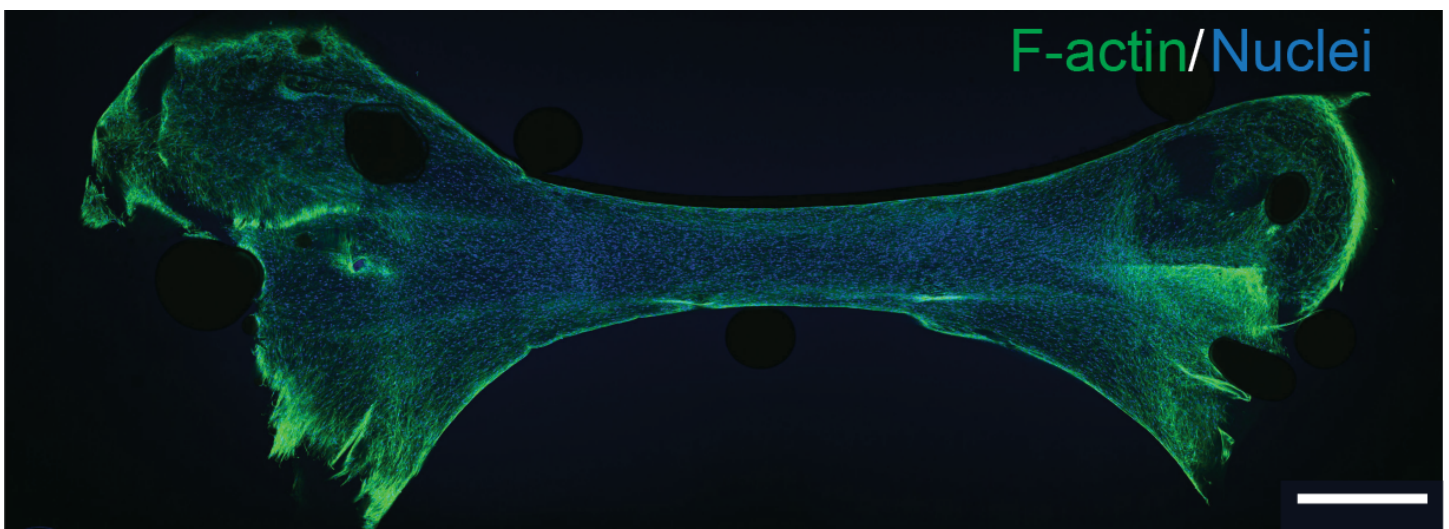


Figure S12. d) Fluorescent image of a patterned PTC stained for F-actin (green) and nuclei (blue). Scale bar is 1 mm.

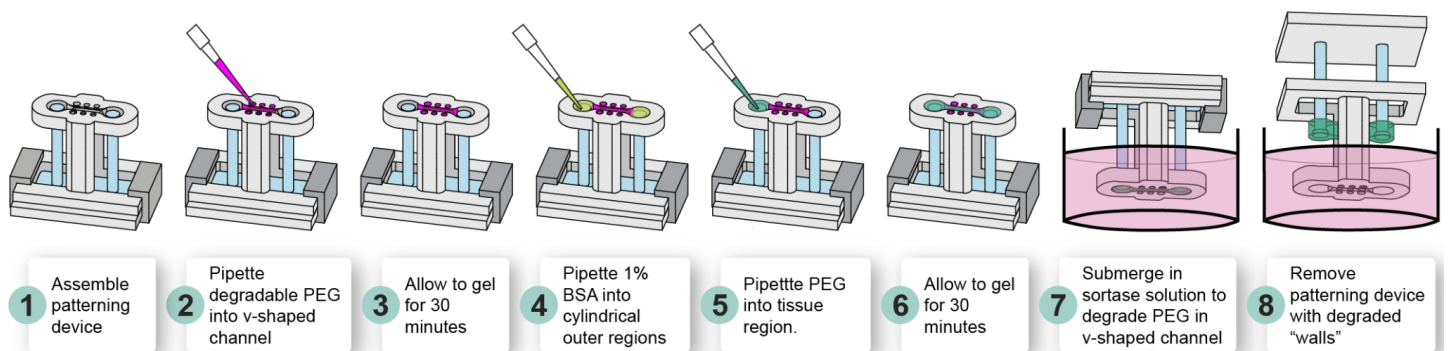


Figure S13. Schematic showing process for patterning a degradable hydrogel channel wall and middle tissue region. The hydrogel depicted in magenta uses a sortase degradable crosslinker allowing for selective degradation of the channel wall with the addition of sortase.

Supplementary Tables

Table S1: Experimental contact angle measurements of 5 mg/mL collagen on 1% BSA treated 3D printed resin

1% BSA treated 3D printed surface number	Contact Angle (degrees)	Average (degrees)	Standard Deviation (degrees)
1	34.73	29.62	2.25
2	28.69		
3	48.41		
4	18.11		
5	26.01		
6	36.31		
7	23.18		
8	20.82		
9	22.38		
10	19.80		
11	41.85		
12	30.75		
13	39.64		
14	35.74		
15	21.75		
16	32.36		
17	39.81		
18	28.28		
19	29.06		
20	14.62		

Table S2. Change in the bulging angle of the pinned fluid's vertical interface as a function of change in volume

w (mm)	h (mm)	ϕ_0 (°)	ϕ_0 (rad)	δ_0 (μm)	S_0 (mm ²)	V_0 (mm ³)	$dV/d\phi$ (mm ³ /rad)	$d\phi/dV$ (°/mm ³)	dV (mm ³)	ϕ (deg)	δ (μm)
0.8	3.5	20	0.35	70.5	0.04	0.13	21.56	2.66	1.0	23	80.1
0.8	3.5	30	0.52	107.2	0.06	0.20	6.93	8.27	1.0	38	138.8
0.8	3.5	40	0.70	145.6	0.08	0.28	3.25	17.66	1.0	57	220.2
0.8	3.5	50	0.87	186.5	0.10	0.36	2.05	27.95	1.0	78	323.6

Table S3: Parameters considered in the vampire and cavity pinning feature design in STOMP

Parameter	Convex “Vampire” Pinning Feature	Concave “Cavity” Pinning Feature
Width between pins, w_1 , w_2 (mm)	0.8	1.2
Vampire angle, α (degrees)	5 to 80	–
Cavity angle, β (degrees)	–	25 to 130
Channel height, h (mm)	3.5	
Collagen density (kg/m ³)	958	
Surface tension (mN/m)	72	
Average static contact angle of collagen on 3D printed resin, θ (degrees)	30 ± 2	
Lowest measured contact angle (degrees)	15	
Highest measured contact angle (degrees)	48	
Gravitation constant (m/s ²)	10	

Supplementary Methods

1. Immunofluorescent imaging of periodontal tissues

PTCs on posts were fixed in 4% PFA at room temperature for 1 hour. PTCs were then dismantled from the posts for the immunofluorescence staining process. In short, PTCs were permeabilized with 0.2% Triton-X for 10 min followed by blocking with 10% normal goat serum (Invitrogen) for 10 min at room temperature. Samples were then incubated for 1 hour with Alexa Fluor 647 phalloidin (Invitrogen A22287, 1:400), and Hoechst 33342 (ThermoFisher, 1:1000). After 1 hour, PTCs were rinsed three times in PBS for 10 min each on a room temperature shaker. Whole PTCs were mounted between glass slides and coverslips using VECTASHIELD mounting medium and allowed to dry overnight. A Leica SP8 confocal microscope was used for imaging. Three to four images per PTC were obtained under 10X objective at 2X zoom and 1024 x 1024 resolution. Since three independent experiments were carried out and each experiment was conducted in triplicate, we ensured a minimum of 30 images per condition for analysis. Laser strength and gain were kept constant between all samples and fields of view (Fig. S12).

2. Synthesis of poly(ethylene glycol)-bicyclononyne (PEG-BCN)

4-arm poly(ethylene glycol)-bicyclononyne (PEG-BCN) was synthesized as described in previous publications¹⁻³. 4-arm poly(ethylene glycol) tetraamine (MW 20kDa, 1.143 g, 0.0571 mmol, 0.2 mol NH₂ groups, 1x; JenKem Technology USA; Plano, TX), (1R,8S,9s)-bicyclo[6.1.0]non-4-yn-9-ylmethyl (2,5-dioxopyrrolidin-1-yl) carbonate (BCN-OSu) (Sigma Aldrich; St. Louis, MO) (100 mg, 0.343 mmol, 1.5x to NH₂ groups), and N,N-Diisopropylethylamine (DIEA, 159 μ L, 8 mmol, 4x to NH₂ groups) were dissolved in anhydrous dimethylformamide (DMF, 5 mL) and stirred overnight. The next day, the mixture was diluted with DI H₂O (10x volume) and dialyzed overnight in DI H₂O (molecular weight cutoff ~ 2kDa; SpectraPor, Repligen; Waltham, MA) and lyophilized over three days to yield a white powder. The powder was resuspended in sterile PBS at a 10 mM stock concentration and stored at -80°C until further use. ¹H NMR confirmed functionalization to be >95% by comparing integral values for characteristic BCN peaks (δ 2.24, 1.57, 1.34, 0.92) with those from the PEG backbone (δ 3.63).

3. Peptide Synthesis of eSrtA(4S9)- and eSrtA(2A9)-sensitive Crosslinkers

The eSrtA(4S9)- and eSrtA(2A9)-sensitive diazide peptide crosslinkers H-RGPQGIWGQLPESGGRK(dde)-NH₂ and H-RGPQGIWGQLAETGGRK(dde)-NH₂, respectively, were synthesized on rink amide ProTide resin (CEM Corporation; Charlotte, NC) following induction heating-assisted Fmoc solid-phase techniques with HCTU activation (Gyros Protein Technologies PurePep Chorus; Tucson, AZ) at a 0.4 mmol scale. Deprotection of the 1-(4,4-dimethyl-2,6-dioxacyclohexylidene)ethyl (dde) group was accomplished by treating with 2% hydrazine monohydrate in DMF (3x10 min). For azide modification of the both the N-terminal amine and the ε-amino group of the C-terminal lysine, 4-azidobutanoic acid (227 μL, 2 mmol, 4x to NH₂ groups), hexafluorophosphate azabenzotriazole tetramethyl uronium (HATU, 750 mg, 1.97 mmol, 3.95x to NH₂ groups) and DIEA (1.38 mL, 8 mmol, 16x to NH₂ groups) were prereacted for 5 minutes and then reacted with the peptide for 1.5 hours. For peptide cleavage and deprotection, the resin was treated with trifluoroacetic acid/triisopropylsilane/water (95:2.5:2.5) for 3 hours, then crashed out and washed in ice-cold diethyl ether (2 x 150mL). The crude peptides were purified via semi-preparative reversed-phase high performance liquid chromatography with a linear gradient of 5-100% acetonitrile and 0.1% TFA for 45 minutes and then lyophilized to yield white powders of the final peptides N₃-RGPQGIWGQLPESGGRK(N₃)-NH₂ and N₃-RGPQGIWGQLAETGGRK(N₃)-NH₂. Peptide mass was verified via ESI-LCMS.

4. eSrtA(4S9) and eSrtA(2A9) Expression and Purification

The pET29B expression plasmids for eSrtA(4S9) and eSrtA(2A9) were a generous gift from Dr. David Liu at Harvard University (Addgene plasmids #75146 and #75145). The sortase variants were expressed and purified as previously described¹. Electrically competent BL21 cells were transfected with the eSrtA(4S9) and eSrtA(2A9) plasmids and selected on kanamycin-containing agar plates. 5 mL of Luria Broth (LB) with kanamycin (50μg/mL) was inoculated with a plasmid-containing colony and grown overnight at 37°C shaking at 200 rpm. The following day, 1 L of LB broth, including 40 mL of autoinduction sugars (60% v/v glycerol, 10% w/v glucose, 8% w/v lactose) as well as kanamycin, was inoculated with the 5mL overnight culture and allowed to incubate at 37°C, 200 rpm overnight. The following day, cells were pelleted via centrifugation (4000g, 20 mins), resuspended in lysis buffer (20 mM Tris, 50 mM NaCl, 10 mM imidazole; pH 7.5) with 1 mM phenylmethylsulfonyl (PMSF; TCI, Portland, OR) protease inhibitor, and lysed by sonication (6x, 3 min cycle, 30% amplitude; Fisher Scientific; Waltham, MA). The lysate was clarified via centrifugation (20 mins, 11000g). The clarified lysate was then purified using an ÄKTA Pure 25 L FPLC (Cytiva; Marlborough, MA) equipped with a 5 mL HisTrap HP column at a flow rate of 5 mL min⁻¹. The column was equilibrated with 5 column volumes (CV) of lysis buffer, followed by loading the sample and washing with 8 CV of endotoxin removal buffer (20 mM Tris, 50 mM NaCl, 20 mM imidazole, 0.1% Triton-X 114; pH = 7.5) and 8 CV of wash buffer (20 mM Tris, 50 mM NaCl, 20 mM imidazole; pH = 7.5). His-tagged protein was eluted over an 8 CV gradient of imidazole (20 mM Tris, 50 mM NaCl, 5-250 mM imidazole; pH = 7.5) into a 96 well plate; protein-containing fractions were pooled and dialyzed with SnakeSkin dialysis tubing (10 kDa cut off; ThermoFisher, Waltham, MA) in PBS over two days. Purified sortase was spin-concentrated using an Amicon Ultra 15 centrifugation filter (10,000 Da cut off; Sigma Aldrich; St. Louis, MO). The final stocks were diluted with PBS containing 10% glycerol to a concentration of 100 μM. Sortase purity was evaluated with sodium-dodecyl sulfate-polyacrylamide gel electrophoresis and identity was confirmed with electrospray ionization mass spectrometry on an AB SCIEX 5600 QTOF instrument (SCIEX; Framingham, MA).

Supplementary Text

1. Full theoretical characterization of pinning in STOMP channels

In this study, we investigate the successive pinning of the two liquids in the STOMP device shown in Fig. S3. The “green” liquid represents a hydrogel (e.g., cell-ECM mixture) first pipetted into the outer cylindrical regions of the STOMP device. The “orange” liquid represents a second hydrogel (cell-ECM mixture) pipetted later in the center region. In this analysis, we assume both hydrogels (green and orange regions) are 5 mg/mL collagen, but this analysis can be extended to any hydrogel by utilizing that specific hydrogel’s properties (e.g., density, contact angle on patterning device surface, etc.).

It is assumed that liquid #1 (green in Fig. S3) is pipetted first, so it is the pinning of this liquid that is investigated here. In a first approach, we follow a 2D approach, neglecting the effect of the horizontal free surfaces at bottom and top. We shall justify this approximation later in the text. Here, we analyze two pinning feature designs we refer to as convex “vampire” pins and concave “cavity” pins.

We first address the case of the convex “vampire” pinning features (Fig. S4). The design is constituted by two facing reliefs resembling two “teeth”. We note that α is the angle formed by the triangular-shaped relief, θ the contact angle of the hydrogel with the channel wall, and w is the distance between the two facing reliefs of the convex “vampire” pins. The Laplace pressure ΔP of the liquid is given by equation (S1), where r is the curvature radius of the pinned interface (in the horizontal plane) and γ denotes the surface tension of the liquid.

$\Delta P = \frac{\gamma}{r}$	(S1)
-------------------------------	------

At the pinning limit (i.e., the maximum interface the fluid bulges before pinning is broken), the bulging fluid front forms the angle θ with the external side of the triangular edge⁴⁻⁸; its complement is noted in Fig. S4. Any additional bulging results in a capillary flow passing over the pinning feature. Let us denote the points A and B the tip of the “teeth”, O the center of the circular arc formed by the interface, and C the middle of the segment AB. Using the construction in Fig. S4, the angle $\{AC, AO\}$ is simply given by the expression $\frac{\pi}{2} - \theta + \frac{\alpha}{2}$. Then considering the rectangular triangle ACO, we find

$\cos\left(\frac{\pi}{2} - \theta + \frac{\alpha}{2}\right) = \frac{w}{2r}$	(S2)
---	------

or

$\sin\left(\theta - \frac{\alpha}{2}\right) = \frac{w}{2r}$	(S3)
---	------

Remark that we have considered $\theta > \frac{\alpha}{2}$. When $\theta = \frac{\alpha}{2}$, the fluid interface is flat and r is infinite. Substituting equation (S3) into equation (S1) yields the threshold Laplace pinning pressure, above which pinning is lost in the convex “vampire” pinning feature design (Eq. S4).

$\Delta P = \frac{\gamma}{r} = \frac{2\gamma \sin\left(\theta - \frac{\alpha}{2}\right)}{w}$	(S4)
--	------

Second, we analyze the case of the concave “cavity” pinning features (Fig. S5). The Laplace pressure is still given by equation (1). Let us note β as the angle of solid at the ridge. Let us separate two cases: $\beta > \theta$ and $\beta < \theta$. The first case is the usual case, because θ is generally small and the cavity angle β cannot be too small due to the 3D printing fabrication process of the STOMP device. The first case ($\beta > \theta$) corresponds to the configuration used here in this work.

Case $\beta > \theta$: Again, at the limit, the bulging angle forms the angle θ with the external side of the tooth⁴⁻⁸; its complement is noted as $\pi - \theta$ in Fig. S5. Any additional bulging results in a capillary flow passing over the ridge. Let us denote the points A and B the tip of the ridges, O the center of the circular arc formed by the interface, and C the middle of the segment AB. Using the construction in Fig. S5, the angle $\{AC, AO\}$ is simply $\beta - \theta$. Then considering the rectangular triangle AC0, we find

$\cos(\theta - \beta) = \frac{w}{2r}$	(S5)
---------------------------------------	------

Substituting equation (S5) into (S1) yields the threshold Laplace pinning pressure, above which pinning is lost in the concave “cavity” pinning feature design (Eq. S6).

$\Delta P = \frac{\gamma}{r} = \frac{2\gamma \cos(\theta - \beta)}{w}$	(S6)
--	------

Case $\beta < \theta$: While this case is not the usual case, we mention it for completion of the study. In this case, the fluid front creates a bulging curvature, where the center of the curvature (point O in Fig. S6) formed is located past the pinning ridge (line segment AB in Fig. S6). The threshold Laplace pinning pressure is still the same as Eq. S5, but this equation reaches its maximum value when β is equal to θ , which is 30° in our theoretical model (the average contact angle of 5 mg/mL collagen on 3D printed resin treated with 1% BSA). Therefore, the maximum Laplace pinning pressure that can be experienced in the concave “cavity” pinning feature is given below in equation (S7) and is visualized as the solid green line in Fig. S6.

$\Delta P = \frac{2\gamma}{w}$	(S7)
--------------------------------	------

Lastly, because gravity has a small, but not negligible effect, we must also consider the hydrostatic pressure at the pinning interface. For both pinning feature designs, the hydrostatic pressure at the bottom of the channel is given below in equation (S8), where ρ is the density of the hydrogel, g is the gravitational constant, and h is the height of the channel.

$\Delta P = \rho gh$	(S8)
----------------------	------

2. Analyzing the 3D effect of gravity in theoretical approach to pinning in STOMP

In our theoretical pinning model for STOMP, we used a 2D approach where we neglected the effect of the horizontal free air-liquid interfaces at the bottom and top of the open channel. To justify this approach, we also analyzed the potential 3D effects, which are twofold: 1) gravity effects that may distort the bottom air-liquid interface of the open channel and 2) corner effects from the rounded vertical air-liquid interface along the height of the open channel.

First, to analyze the effect of gravity, the Bond number has to be calculated. For testing the pinning in STOMP, devices with a channel height of 3.5 mm and width of 1.2 mm were used. The equation for bond number Bo is given below in equation (S9), where ρ is the density of the 5 mg/mL collagen hydrogel, g is the gravitational constant, h is the height of the channel, R is the radius of the outer cylinders, and γ is the surface tension of the liquid (estimated to be water here).

$Bo = \frac{\rho ghR}{\gamma}$	(S9)
--------------------------------	------

In the case of the outer cylinders, the radius is 1.5 mm. Therefore, the bond number for the outer cylinders can be approximately calculated, as shown below in equation (S10).

$Bo_{outer\ cylinders} = \frac{958 \frac{kg}{m^3} \cdot 10 \frac{m}{s^2} \cdot 3.5 \cdot 10^{-3} m \cdot 1.5 \cdot 10^{-3} m}{72 \cdot 10^{-3} \frac{N}{m}} \approx 0.7$	(S10)
--	-------

In the case of the central region of the open channel, the radius R is replaced by the semi-width, $w/2$. When experimentally testing the pinning, we used the STOMP devices with a channel height of 3.5 mm and a width of 1.2 mm. Therefore, the bond number for the central region can be approximately calculated with a semi-width of 0.6 mm, as shown below in equation (S11).

$Bo_{central\ region} = \frac{958 \frac{kg}{m^3} \cdot 10 \frac{m}{s^2} \cdot 3.5 \cdot 10^{-3} m \cdot 0.6 \cdot 10^{-3} m}{72 \cdot 10^{-3} \frac{N}{m}} \approx 0.3$	(S11)
---	-------

In both cases of the outer cylinders that surround the posts and the central region of the open channel where flow occurs, we calculated that $Bo < 1$, which means surface tension forces dominates in the open channel. In both cases, gravity has a small effect on the horizontal free air-liquid interface at the bottom and top of the open

channel. While the effect of gravity is not negligible, it is small enough that we can justify using a 2D approach in our theoretical characterization of the pinning in the STOMP devices.

The corner effects of the vertical air-liquid interface along the height of the open channel are more difficult to predict. We used Brakke's software Surface Evolver to determine the shape of these interfaces⁹. The results are plotted in Fig. S7, which demonstrates that some corner effects do exist in our STOMP system.

3. Experimentally testing different volumes and pinning feature angles in STOMP

To understand the sensitivity of our system to changes in volume, we tested pinning in five different pinning angles of both pinning feature designs (i.e., $\alpha=10^\circ, 20^\circ, 30^\circ, 45^\circ,$ and 60° for the convex "vampire" pins and $\beta=40^\circ, 60^\circ, 90^\circ, 100^\circ,$ and 120° for the concave "cavity" pins, $n=3$ devices for each pin angle) at four different volumes (20, 22, 23, and 24 μL). These results are illustrated in Fig. S2.

Every volume tested exhibited different pinning results, where increasing the volume resulted in less successful pinning. At every volume, the concave "cavity" pinning feature with pins $\beta=120^\circ$ resulted in failed pinning; this matches what we would expect from the theoretical results (see Fig. 2d). Generally, in all volumes tested, the concave "cavity" pinning feature was more consistent than the convex "vampire" pinning feature. This phenomenon may be explained by the large range in the pinning Laplace pressure for the convex pinning features (see Fig. 2c). We observed that a volume of 23 μL best fitted our theoretical model.

When 23 μL was pipetted into the convex "vampire" pinning features, we observed successful pinning of the collagen solution when $\alpha=10^\circ, 20^\circ, 30^\circ$ ($n=3/3$ devices pinned). These experimental results match what would be expected from the average theoretical maximum Laplace pinning pressure (Fig. 2c). Further, there was less successful pinning when $\alpha=45^\circ$ and 60° ($n=2/3$ devices did not pin). We note that one out of the three devices for both the angles $\alpha=45^\circ$ and 60° had successful pinning, but these angles have conditions of success and failure within the pinning range of the maximum Laplace pinning pressure (Fig. 2c, green shading showing successful conditions and magenta shading showing failure conditions), suggesting that those devices had variable BSA adsorption onto the channel walls that may have changed the contact angle of the collagen on the channel surface.

When 23 μL was pipetted into the concave "cavity" pinning features, we observed successful pinning of the collagen solution when $\beta=40^\circ$ and 60° ($n=3/3$ devices pinned) and no pinning when $\beta=90^\circ, 100^\circ,$ and 120° ($n=3/3$ devices did not pin). While successful pinning at $\beta=40^\circ$ and 60° experimentally matches the theory, loss of pinning was observed in all three replicates in devices with $\beta=90^\circ$ which was expected, even within the contact angle range, to successfully pin (Fig. 2d). It is possible that the contact angle was towards the lower bound of the possible threshold Laplace pressure (Fig. 2d), where the line does cross below the hydrostatic pressure at $\beta=90^\circ$. There could also be additional reasons for fluid de-pinning when not predicted. In some cases, a fluid may initially pin, but then lose that pinning if there are deformities present on the pinning feature (i.e., rough surface, inconsistency in 3D printing, etc.).

4. Influence of liquid volume in pinning

Since we observed differences in pinning as the pipetted volume changed, we wanted to look at two possible factors that could influence pinning: 1) change in the horizontal interface of the liquid in the channel (i.e., change in volume of liquid bulging at the top and bottom of the channel) and 2) change in the vertical interface of the pinned fluid front (i.e., change in the pinned fluid angle).

First, we will estimate the volume bulging at the bottom of the channel due to the weight of the precursor liquid hydrogel in the STOMP channel. At the bottom of the channel, the air-liquid interface bends due to hydrostatic pressure, as depicted in Fig. S8. If we consider the bending of the horizontal bottom surface to be a cylinder, then the curvature of the surface is $\kappa = 1/R$. Therefore, the bending of the surface by hydrostatic pressure can be modeled by equation (S12), where R is the curvature radius of the bulging surface.

$\Delta P = \rho g h = \frac{2\gamma}{R}$	(S12)
---	-------

If a denotes the radius of the cylinder, the volume of the liquid in the spherical cap bulging below the cylinder is given below in equation S13.⁴

$$V_{horizontal\ bulging} = \frac{\pi}{6} (R - \sqrt{R^2 - a^2}) [3a^2 + (R - \sqrt{R^2 - a^2})^2] \quad (S13)$$

From Berthier and Brakke⁴, the negative bulging height can be deduced as

$$R = \frac{a^2 + h^2}{2h} \quad (S14)$$

or

$$h = R - \sqrt{R^2 - a^2} \quad (S15)$$

If ρ is 958 kg/m³ (density of 5 mg/mL collagen), g is 9.8 m/s², h is 3.5 mm (the height of the open channel), γ is 72 mN/m, and a is 1.5 mm (the radius of the outer cylinders of the STOMP device), then we find that the curvature radius R is 4.38 mm, giving a bulging volume of 0.945 μ L (or 0.945 mm³) with a bulging height of 0.265 mm (or 265 μ m). Thus, if the volume of the precursor hydrogel is equal to exactly the volume of the cylinder plus the inner channel walls (unto the pinning features), then the bottom surface bulges out 265 μ m below the channel.

Next, we will calculate the surface area of the pinned fluid's vertical interface as a function of the pinning angle. Figure S9 shows a top-down cross section of the STOMP channel, where R is the curvature radius of the bulging vertical interface, w is the width of the open channel, δ is the bulging distance of the pinned fluid's vertical interface, ϕ is the pinning angle of the fluid front, and S is the vertical surface denoted with a dark green line. In a 2D approximation, a change in volume delimited by the surface S can be modeled as

$$V_{vertical\ bulging} = h \cdot S \quad (S16)$$

where h is the height of the open channel. Geometrical considerations give us the curvature radius R , denoted below in equation (S17).

$$R = \frac{w}{2\sin(\phi)} \quad (S17)$$

Modeling the vertical bulging surface as a circular segment, the surface area of the arc (denoted as S) can be modeled by equation (S18).

$$S = \frac{R^2}{2} [2\phi - \sin(2\phi)] \quad (S18)$$

Substituting equation (S17) and (S18) into (S16), we obtain an equation that calculates the change in volume of the vertical surface S as a function of the bulging pinning angle ϕ .

$$V_{vertical\ bulging} = h \cdot \frac{R^2}{2} [2\phi - \sin(2\phi)] = h \cdot \frac{w^2}{8} \frac{2\phi - \sin(2\phi)}{\sin^2(\phi)} \quad (S19)$$

Additionally, the bulging distance δ is given by equation (S20).

$$\delta = R[1 - \cos(\phi)] = \frac{w(1 - \cos\phi)}{2\sin(\phi)} \quad (S20)$$

As more liquid is added to the channel, the vertical interface of the pinned fluid will continue to bulge past the pinning features, thus changing the angle of the pinned liquid. Let us now assume that an additional liquid volume, denoted as dV , is added to the initial volume V (Fig. S10). The surface area of the vertical interface now becomes $S + dS$. To find the effect of the increase of volume dV on the bulging angle ϕ , we can calculate the derivative of equation (S19) to find $dV/d\phi$. This derivatization gives us equation (S21)

$\frac{dV}{d\phi} = h \frac{w^2 [\sin(\phi) + 2\phi + \cos(3\phi)]}{4 \sin^3(\phi)}$	(S21)
--	-------

which gives us $d\phi/dV$ in equation (S22).

$\frac{d\phi}{dV} = \frac{4\sin^3(\phi)}{hw^2[\sin(\phi) + 2\phi + \cos(3\phi)]}$	(S22)
---	-------

The values of the increased bulging angle ϕ with an increase of liquid volume of only 1 μL (or 1 mm^3) for 4 initial pinning angles ϕ_0 (20°, 30°, 40°, and 50°) are listed in Table S2. We find that adding 1 μL of additional volume can change the bulging angle; for example, an initial pinning angle of 40° or 50° can increase by 17° or 28°, respectively, with the addition of only 1 μL . This calculation can help explain why experimentally we observed changes in successful pinning of the fluid front at different pipetted volumes.

REFERENCES

1. Bretherton, R. C. *et al.* User-Controlled 4D Biomaterial Degradation with Substrate-Selective Sortase Transpeptidases for Single-Cell Biology. *Adv. Mater.* **35**, 2209904 (2023).
2. DeForest, C. A. & Tirrell, D. A. A photoreversible protein-patterning approach for guiding stem cell fate in three-dimensional gels. *Nat. Mater.* **14**, 523–531 (2015).
3. Kopyeva, I. *et al.* Stepwise Stiffening/Softening of and Cell Recovery from Reversibly Formulated Hydrogel Double Networks. Preprint at <https://doi.org/10.1101/2024.04.04.588191> (2024).
4. Berthier, J. & Brakke, K. A. Sessile Droplets. in *The Physics of Microdroplets* 105–142 (Wiley, 2012). doi:10.1002/9781118401323.
5. Buguin, A., Talini, L. & Silberzan, P. Ratchet-like topological structures for the control of microdrops. *Appl. Phys. A* **75**, 207–212 (2002).
6. Ondarçuhu, T. Total or Partial Pinning of a Droplet on a Surface with a Chemical Discontinuity. *J. Phys. II* **5**, 227–241 (1995).
7. Bico, J., Marzolin, C. & Quéré, D. Pearl drops. *Europhys. Lett. EPL* **47**, 220–226 (1999).
8. Bico, J., Tordeux, C. & Quéré, D. Rough wetting. *Europhys. Lett. EPL* **55**, 214–220 (2001).
9. Brakke, K. A. The Surface Evolver. *Exp. Math.* **1**, 141–165 (1992).